

Contrasting thermodynamic and hydrodynamic entropy

Mahendra K. Verma,^{1,*} Rodion Stepanov,^{2,3,†} and Alexandre Delache^{4,5,‡}

¹*Department of Physics, Indian Institute of Technology Kanpur, Kanpur 208016, India*

²*Institute of Continuous Media Mechanics, Korolyov 1, 614013, Perm, Russia*

³*Perm National Research Polytechnic University, Komsomolskii av. 29, 614990 Perm, Russia*

⁴*Ecole Centrale de Lyon, CNRS, Universite Claude Bernard Lyon 1, INSA Lyon, LMFA, UMR5509, 69130, Ecully, France*

⁵*Jean Monnet University, 42100 Saint-Étienne, France*

(Dated: December 6, 2024)

In this paper, using *hydrodynamic entropy* we quantify the multiscale disorder in Euler and hydrodynamic turbulence. These examples illustrate that the hydrodynamic entropy is not extensive because it is not proportional to the system size. Consequently, we cannot add hydrodynamic and thermodynamic entropies, which measure disorder at macroscopic and microscopic scales, respectively. In this paper, we also discuss the hydrodynamic entropy for the time-dependent Ginzburg-Landau equation and Ising spins.

I. INTRODUCTION

The universe is a fascinating mix of order and disorder. For example, the paramagnet transforms to a ferromagnet below the critical temperature. Thermodynamic entropy (TE in brief) quantifies disorders in these systems. Boltzmann [1] and Gibbs [2] showed that TE has a microscopic origin, and it is related to the configurations of spins and atoms of the system [3]. The microscopic entropy is often referred to as Boltzmann entropy, *BE* in short. The phase transitions in such systems have been explained using equilibrium statistical physics [3–5]. For example, a ferromagnet has a long-range order (LRO), with a nonzero average of the order parameter [3]. Refer to Appendix A for a brief discussion on TE, BE, and Gibbs entropy.

Nonequilibrium systems have another kind of disorder. For example, the correlations of the order parameter (here, velocity field) in thermal-convection rolls [6], Jupiter’s red spot, and Earth’s Hadley shells [7] are dynamic, and they differ from those in a equilibrium systems. A typical route to turbulence in nonequilibrium systems follows the following path: instability, pattern formation, spatio-temporal chaos, and then turbulence [8]. In the following discussions we show that BE is inadequate for describing disorder in nonequilibrium systems. Instead, *hydrodynamic entropy* (HE in short) [9] is a quantifier for the disorder in a variety of nonequilibrium systems.

In the following discussion we focus on the disorder in nonequilibrium multiscale systems, namely in *Euler turbulence* and in *thermal convection*. Variations in TE is proportional to the heat production, which is absent in an Euler flow due to lack of viscosity. Therefore, TE of an Euler flow is constant [10]. However, Euler flow exhibits a

nontrivial temporal evolution and finite energy flux when the flow starts with large-scale structures [11]. In a recent work, Verma and Chatterjee [9] showed that HE describes the disorder in Euler turbulence quite well. For an ordered initial condition, 3D Euler equation evolves from order to disorder or HE increases with time. However, for several coherent initial conditions, 2D Euler turbulence becomes more ordered with time, or HE decreases for a finite time duration. Thus, HE provides valuable insights and quantitative descriptions for Euler turbulence.

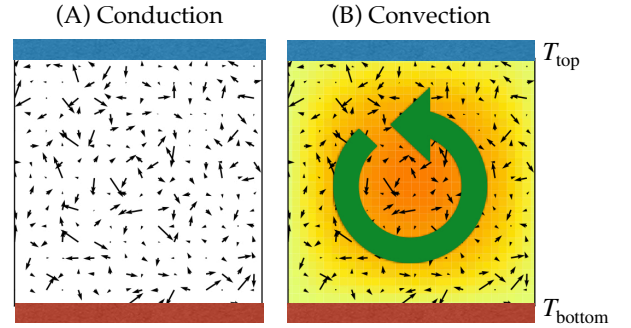


FIG. 1. A box of ideal gas is being heated from below and cooled from top. Here we illustrate the velocities of the molecules for (A) Conduction state and (B) Convection state. In (A), the molecules move with random thermal speed, whereas in (B) the molecules have an additional velocity due to the convection roll. The convection state is more ordered than the conduction state; this contrast can be quantified using hydrodynamic entropy.

Now we turn to thermal convection, for which Prigogine provided valuable insights in terms of dissipative structures [12]. Here, a fluid is confined between two plates, with the bottom plate at T_{bottom} and the top plate at T_{top} , and $T_{\text{bottom}} > T_{\text{top}}$. See Fig. 1 for an illustration. For a temperature difference $(T_{\text{bottom}} - T_{\text{top}})$ below a critical value $(\Delta T)_c$, heat is transported by conduction

* mkv@iitk.ac.in

† rodion@icmm.in

‡ alexandre.delache@ec-lyon.fr

in the stationary fluid. However, convective rolls are born when the temperature difference exceeds $(\Delta T)_c$. A typical convection experiment with air has the temperature difference varying from 10 to 100 Celsius. In such a system, the hydrodynamic velocity of the convection rolls is $O(1 \text{ cm/s})$, which is much smaller than the thermal speed ($\sim 300 \text{ m/s}$). As shown in Fig. 1, the molecules in the conduction state move randomly with the thermal velocity, whereas the molecules in the convection state have an additional hydrodynamic (coherent) velocity, which is much smaller than the thermal speed.

Near the onset of convection, the average temperatures of the conduction and convection states are nearly the same, leading to approximately similar Boltzmann entropies (BEs) for the two configurations [see Eq. (A1)]. BE describes the disorder for the conduction state quite well, but it fails to capture the order of the convective roll [see Fig. 1(B)]. Similar features exist in Earth's atmosphere too. Here, the hydrodynamic velocity, which is $O(1 \text{ m/s})$, is much smaller than the thermal speed. These observations mandates construction of a new formula to quantify the hydrodynamic order. Prigogine [13] highlights this aspect as follows, “the canonical distribution would assign almost zero probability to the occurrence of Bénard convection. Whenever new coherent states occur far from equilibrium, the very concept of probability, as implied in the counting of number of complexions, breaks down”. As we show in this paper, the framework of *hydrodynamic entropy* overcomes this deficiency of equilibrium statistical mechanics.

Quantification of disorder and correlations in biological, economic, and social systems remains a challenge. However, there are interesting applications of Shannon's entropy [14] to cities, ecology, and income distributions [15–18]. Other leading applications of entropy measures include electroencephalogram (EEG) [19], electrocardiogram (ECG) [20], and chaos [21]. Interestingly, most of the above systems—cities, finance, income distribution, EEG, ECG—are multiscale, for which HE could provide valuable measures and insights. In fact, some works on EEG [19], ECG [20], and chaos theory [21] employ Fourier transforms, as in HE, for entropy quantification.

In this paper, we define HE, contrast it with thermodynamic entropy, and then employ HE to variety of systems—Euler turbulence, hydrodynamic turbulence, Ising spins, and coarsening. The *hydrodynamic entropy maxima* of Euler turbulence and Ising spins are proportional to the logarithms of the respective grid sizes, indicating that HE is nonextensive. We show that the HE of hydrodynamic turbulence is between 3 and 4, and it is independent of the grid size. Our results appear quite general and illuminating, and we expect similar results to hold for other nonequilibrium systems.

The outline of the paper is as follows. We define hydrodynamic entropy in Section II, and compute hydrodynamic entropies for Euler and fluid turbulence in Sections III and IV respectively. Section V discusses the

hydrodynamic entropies for the Ising spins and time-dependent Ginzburg-Landau equation. We conclude in Section VI. In Appendix A, we summarize the Boltzmann entropy, Gibbs entropy, Shannon entropy, von Neumann entropy, and Tsallis entropy in order to compare them with hydrodynamic entropy.

II. DEFINITION OF HYDRODYNAMIC ENTROPY

In this section, we define hydrodynamic entropy (HE), which is primarily suitable for multiscale nonequilibrium systems [9, 22]. The hydrodynamic entropy is computed using the energy spectrum as follows. For a scalar quantity ψ , the modal energy is defined as

$$E(\mathbf{k}) = \frac{1}{2} |\psi(\mathbf{k})|^2, \quad (1)$$

where $\psi(\mathbf{k})$ is the Fourier transform of $\psi(\mathbf{x})$. The corresponding modal energy for vector field (e.g., velocity field) \mathbf{u} is

$$E(\mathbf{k}) = \frac{1}{2} |\mathbf{u}(\mathbf{k})|^2. \quad (2)$$

Nonequilibrium systems driven at large scales create structures with different energies, among which the large-scale structures dominate the order or correlations. Following this idea, Verma and Chatterjee [9] proposed that the probability $p_{\mathbf{k}}$ for wavenumber \mathbf{k} is proportional to its modal energy $E(\mathbf{k})$. That is,

$$p_{\mathbf{k}} = \frac{E(\mathbf{k})}{\sum_{\mathbf{k}} E(\mathbf{k})} \quad (3)$$

with $\sum_{\mathbf{k}} p_{\mathbf{k}} = 1$, and HE is

$$S_H = - \sum_{\mathbf{k}} p_{\mathbf{k}} \log_2 p_{\mathbf{k}}. \quad (4)$$

In this measure, larger the energy of a mode, larger its contribution to the HE. For isotropic systems, as in isotropic hydrodynamic turbulence, $E(\mathbf{k})$ depends on k . For such systems, we redefine $p_{\mathbf{k}}$ and S_H of Eqs. (3, 4) as follows:

$$p_k = \frac{E(k)}{\sum_k E(k)}, \quad (5)$$

$$S_H = - \sum_k p_k \log_2 p_k, \quad (6)$$

where $E(k) = \sum_{k-1 < |\mathbf{k}'| \leq k} E(\mathbf{k}')$ is the shell spectrum for unit-width shell of radius k . Equations (5, 6) lead to considerable simplification in the computation of S_H for isotropic systems. Interestingly, HE can be computed for a given snapshot, a convenient feature using which we can compute the entropy time series for a system.

Thus, HE can yield valuable insights into the evolution of dynamical systems.

Let us contrast HE with the thermodynamic entropy (TE) or Boltzmann entropy (BE). Application of BE hinges on the *a priori probability postulate* and *ergodic hypothesis* of statistical mechanics [3]. Classical and quantum statistical mechanics typically deal with Hamiltonian systems whose energies are conserved. We consider a closed system with N interacting particles that moves in $6N$ dimensional phase space. A *microstate* of the system contains information on the positions and velocities of all the particles, but a *macrostate* is a combination of many microstates with similar configurations. Boltzmann related the thermodynamic entropy to all the microstates for a given macrostate [1, 23]. See Appendix A.

It is conjectured that the systems of statistical mechanics reach thermal equilibrium, or *thermalize*, asymptotically. According to *ergodic hypothesis*, a system under equilibrium covers the available phase space (satisfying energy conservation) such that the temporal average of a quantity equals its ensemble average. Intuitively, the *a-priori probability postulate* originates from this observation. In addition, in the equilibrium state, BE is maximum, and the energy is equipartitioned among all the modes. Proving that a system is ergodic is quite complex, but it is much simpler to show thermalization for a system. In this context, Cichowlas *et al.* [11] showed that three-dimensional (3D) Euler turbulence (energy conserving system) reaches equilibrium asymptotically. However, for some initial conditions, two-dimensional (2D) Euler turbulence does not reach equilibrium [9]. Using numerical simulations, Orszag [24] analyzed a five-mode energy conserving model, resembling Euler equation, and showed that this model thermalizes and becomes ergodic. Thus, behaviour of the Euler equation is both consistent and inconsistent depending on the initial condition.

Note, however, that many natural systems are driven and dissipative. Hence, the validity of the thermalization conjecture remains uncertain for such systems. The total energy is not conserved in such systems, but it fluctuates around the system's steady-state average [25]. In addition, the energy is typically concentrated at large scales, rather than being equipartitioned among the available modes. Thus, nonequilibrium steady states are very different from the equilibrium states of statistical mechanics.

As we show later in this paper, HE is more appropriate than BE for quantifying order in nonequilibrium systems. In Rayleigh-Bénard convection, the convection rolls contribute to the HE. In driven-dissipative nonequilibrium system—turbulence, earthquakes, financial market, galaxies—the energy decreases when we go from large scales to small scales [25, 26]. The disorder in such systems can be satisfactorily quantified using HE, as we show in subsequent sections of this paper.

Note, however, that some unforced and dissipation-less

hydrodynamic systems, e.g., Euler equation, reach equilibrium where the total energy is equipartitioned among all the available Fourier modes; the equilibrium state has the maximum HE. We also show that unlike BE, HE is not extensive.

In the following sections we will compute HE for Euler and hydrodynamic turbulence, the Ising spins, and ϕ^4 theory. Using these examples, we will contrast HE with TE. For example, we illustrate that HE is nonextensive.

III. HYDRODYNAMIC ENTROPY FOR EULER TURBULENCE

Euler equation that describes fluid flow with zero viscosity and no external force is [27–29]

$$\frac{\partial \mathbf{u}}{\partial t} + \mathbf{u} \cdot \nabla \mathbf{u} = -\nabla p, \quad (7)$$

where \mathbf{u}, p are the velocity and pressure fields respectively. We assume the fluid to be incompressible ($\nabla \cdot \mathbf{u} = 0$). For an ordered initial condition (e.g., Taylor-Green vortex), 3D Euler turbulence evolves from order to disorder, and it reaches an equilibrium state asymptotically [11]. But, the thermodynamic entropy (TE) of this system remain constant due to an absence of viscosity or heat production [10]. Note that Euler equation does not include any thermal or dissipative component, as in Navier-Stokes equation (see Sec. IV). Due to these reasons, TE cannot capture the above variations in the disorder. As we illustrate below, HE successfully captures the evolution towards disorder in Euler turbulence [9].

Lee [27] and Kraichnan [28] derived the equilibrium solutions of Euler turbulence. In the absence of *kinetic helicity* ($\mathbf{u} \cdot (\nabla \times \mathbf{u})$), the velocity correlation in the equilibrium state is delta-correlated in space and time that leads to statistical equipartition of energy among all the Fourier modes [30]. Euler turbulence is often simulated using a finite grid in Fourier space, hence it is also referred to as *truncated Euler turbulence*. If G is the number of grid points in each direction, then the total number of grid points in 3D is $M = G^3$. Since the energy is equipartitioned,

$$\langle E(\mathbf{k}) \rangle = \frac{1}{2} \langle |\mathbf{u}(\mathbf{k})|^2 \rangle = \text{const}, \quad (8)$$

which leads to

$$p_{\mathbf{k}} = \frac{\langle E(\mathbf{k}) \rangle}{\sum_{\mathbf{k}} E(\mathbf{k})} = \frac{1}{M}. \quad (9)$$

Therefore, using Eq. (4) we derive the HE of the equilibrium state as

$$S_H = \sum \frac{1}{M} \log_2 M = \log_2 M. \quad (10)$$

For ordered initial conditions, 3D Euler flows evolve from order to disorder. The asymptotic state of 3D Euler

turbulence has the maximum entropy, which is $\log_2 M$, but the intermediate states have HE less than $\log_2 M$. The evolution for 2D Euler turbulence is more complex. Random delta-correlated initial conditions lead to equilibrium states with maximum HE, but some ordered initial conditions yield nonequilibrium asymptotic states, for which HE decreases for some duration (or the system becomes more ordered) [9].

As shown in Eq. (10), the maximum HE of Euler turbulence is proportional to $\log_2 M$, not to M , as in the BE of Ising spin (see Appendix A). Hence, HE is not proportional to the system size. Therefore, the HE of Euler turbulence is nonextensive. We remark that the dissipation-less Burgers and Korteweg–De Vries (KdV) equations exhibit similar properties [31]. That is, they approach equilibrium states whose HE is proportional to $\log_2 M$, where M is the grid size.

Thus, HE successfully captures the disorder in Euler turbulence. In contrast, the TE remains constant during its evolution.

IV. HYDRODYNAMIC ENTROPY OF A TURBULENT FLOW

The incompressible Navier-Stokes equation, an extension of Euler equation with kinematic viscosity ν and external force \mathbf{F}_{ext} , is

$$\frac{\partial \mathbf{u}}{\partial t} + \mathbf{u} \cdot \nabla \mathbf{u} = -\nabla p + \nu \nabla^2 \mathbf{u} + \mathbf{F}_{\text{ext}}. \quad (11)$$

We assume the density of the fluid to be unity. The above equation exhibits turbulent behaviour for large Reynolds number $\text{Re} = UL/\nu$, where U, L are the large-scale velocity and length scales respectively. In this section, we will compute the hydrodynamic entropy of a turbulent flow.

In a turbulent system, fluid structures contribute to the *coherent hydrodynamic energy*, whereas molecular motion at the microscopic scales contribute to the *incoherent thermal energy*. Here, the large-scale hydrodynamic energy cascades to small scales, where the hydrodynamic energy is converted to the thermal energy of the molecules [25]. Thus, the fluid gets hotter at the expense of hydrodynamic energy of the flow. The TE captures the disorder at the microscopic scales, whereas HE captures the macroscopic disorder of the hydrodynamic structures.

In the following discussion, we *estimate* the HE of a turbulent flow that follows Kolmogorov's energy spectrum [25, 32], i.e.,

$$E(k) = K_{\text{Ko}} \epsilon^{2/3} k^{-5/3}, \quad (12)$$

where ϵ is the energy flux, and K_{Ko} is Kolmogorov's constant. The derivation of HE is simplified when we divide the wavenumber sphere into logarithmically-binned G shells. Since Kolmogorov's theory of turbulence follows a powerlaw, we divide the wavenumber sphere into

shells whose radii k_n 's are given by

$$k_n L = \lambda^n, \quad (13)$$

where n (ranging from 1 to G) is the shell index, L is the box size, and λ is a parameter which is greater than 1. For simplicity, we ignore the dissipation range, and assume the minimum and maximum shell indices to be 1 and G respectively. The energy of the n^{th} shell is

$$E_n = K_{\text{Ko}} \int_{k_n}^{k_{n+1}} dk \epsilon^{2/3} k^{-5/3} \approx \frac{3}{2} K_{\text{Ko}} \epsilon^{2/3} k_n^{-2/3} [1 - \lambda^{-2/3}]. \quad (14)$$

We simplify our calculation by setting $(3/2)K_{\text{Ko}}[1 - \lambda^{-2/3}] \approx 1$ that leads to

$$E_n = \epsilon^{2/3} k_n^{-2/3}. \quad (15)$$

The above spectrum is similar to that in the *shell model* [33, 34]. Similarly, the total kinetic energy of the system is approximately

$$E = \int_{k_0}^G dk E(k) \approx \int_{k_0}^{\infty} dk E(k) \approx \epsilon^{2/3} L^{2/3}. \quad (16)$$

We estimate the probability p_n using

$$p_n = \frac{E_n}{E} = A(k_n L)^{-2/3} = A\lambda^{-\alpha n}, \quad (17)$$

where $\alpha = 2/3$, and A is the prefactor, which is chosen so as to conserve probability. We have lumped the prefactors of earlier equations into A . The constraint $\int dp_n = 1$ yields

$$A = 1 / \int_1^G dn \lambda^{-\alpha n} = \frac{\alpha \ln \lambda}{\lambda^{-\alpha} - \lambda^{-\alpha G}}. \quad (18)$$

The choice of k_n of Eq. (13) plays an important role in making the constant A dimensionless. For a linearly spaced k_n , the probability $p_n = D(k_n L)^{-2/3}/k_n$, where D is a constant with dimension L^{-1} . Thus, logarithmically-binned shells simplify our S_H computation significantly.

Using p_n of Eq. (17), we compute the hydrodynamic entropy as

$$\begin{aligned} S_H &= - \sum_n p_n \log_2 p_n \\ &\approx - \int_1^G dn p_n \log_2 p_n \\ &= - \int_1^G dn A \lambda^{-\alpha n} [\log_2 A - \alpha n \log_2 \lambda] \\ &= \left[A \frac{\log_2 \lambda}{\ln \lambda} - A \log_2 A \right] \left[\frac{\lambda^{-\alpha} - \lambda^{-\alpha G}}{\alpha \ln \lambda} \right] \\ &\quad + \frac{\log_2 \lambda}{\ln \lambda} A \lambda^{-\alpha G} (1 - G). \end{aligned} \quad (19)$$

In the limit $G \rightarrow \infty$, $A \rightarrow \lambda^\alpha \ln(\lambda^\alpha)$ that leads to

$$S_H \rightarrow \frac{\log_2 \lambda}{\ln \lambda} - \log_2(A) = \frac{\log_2 \lambda}{\ln \lambda} - \log_2[\lambda^\alpha \ln(\lambda^\alpha)]. \quad (20)$$

Note that $\alpha = 2/3$ for hydrodynamic turbulence. For this α , in Fig. 2(a) we plot $S_H(G)$ as a function of G for $\lambda = 1.2, 1.3, 1.4$, and 1.5 . As shown in the figure, S_H increases monotonically and approaches a constant. The asymptotic S_H for $\lambda = 1.2, 1.3, 1.4, 1.5$ are 4.31, 3.71, 3.26, 2.94 (approximately) respectively. Note that S_H is nearly constant for $G > 20$. This is because p_n drops very sharply with n , implying that S_H gets maximal contributions from small n 's or large-scale structures only. Note the marginal variations in S_H with λ . Hence, the choice of λ is arbitrary, as in the shell model [33, 34].

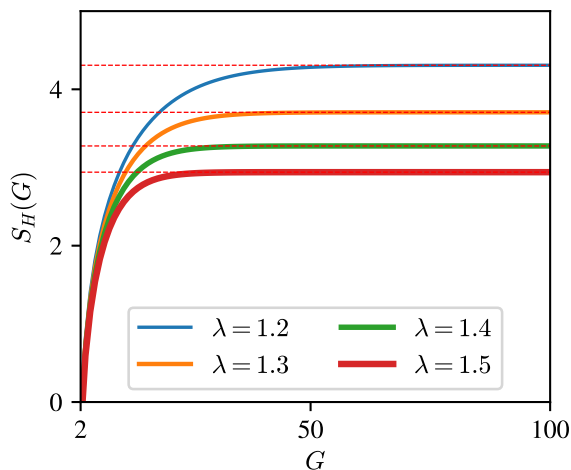


FIG. 2. Plots of hydrodynamic entropies computed using the analytical formula [Eq. (19)] for $\alpha = 2/3$ and $\lambda = 1.2, 1.3, 1.4, 1.5$ using colored lines of increasing thicknesses. The asymptotic values [Eq. (20)] for the four λ 's are 4.31, 3.71, 3.26, and 2.94 respectively (shown using horizontal dashed lines).

We compare the analytical estimates derived above with S_H computed using simulation data. Using pseudospectral code TARANG [35], we simulate hydrodynamic turbulence on a periodic $(2\pi)^3$ box with 512^3 grid points. We choose the nondimensional kinematic viscosity as $\nu = 10^{-3}$. Using the scheme described in Sadhukhan *et al.* [36], we employ random force at low wavenumbers with kinetic-energy supply rate $\epsilon = 0.1$, and zero kinetic-helicity supply rate. We time advance the Fourier modes using fourth-order Runge-Kutta (RK4) method with a time-step $dt = 10^{-3}$. For the time stepping, we absorb the viscous term using exponential integrating factor [37, 38].

We start our simulation with a turbulent initial condition given by Pope [25]. After around 7 eddy turnover times, the system reaches a steady state, whose Reynolds

number Re based on system size is approximately 5580. The Reynolds number based on Taylor's microscale (Re_λ) is approximately 230. Our simulation is well resolved because $k_{\max}\eta \approx 1.25$, where $\eta = (\nu^3/\epsilon)^{1/4}$ is the Kolmogorov length. Figure 3(A) exhibits the energy spectrum $E(k)$ for $t = 0.1, 0.2, 1.0$, and 12.5 eddy turnover times. In the figure, a narrow wavenumber range [$k = (5, 30)$] exhibits $k^{-5/3}$ spectrum, which is shown as a purple dashed curve.

As shown in Fig. 3(A), $E(k)$ at higher wavenumbers grow initially, after which $E(k)$ saturates to a steady profile [25]. The above increase in $E(k)$ at large k 's leads to an increase in S_H in the early stages [Fig. 3(B)]. However, S_H saturates to a near constant value (≈ 3.8) after $t = 7.5$ eddy turnover times. The asymptotic S_H for the simulation is near S_H for $\lambda = 1.3$. A cautionary remark, the definitions of probability (p_n) for the analytical and numerical calculations are somewhat different. However, the sums leading to S_H yield nearly the same results because all the modes have been accounted for in both sums. The difference arising due to log-binned shells is marginal. Note that the Boltzmann entropy computations too involve large sums where we ignore marginal terms.

Thus, using analytical and numerical tools we show that the HE of hydrodynamic turbulence is nearly constant, independent of grid size. Hence, *HE of a turbulent system is nonextensive*. Interestingly, S_H for hydrodynamic turbulence is smaller than that for the disordered Euler turbulence [Eq. 10]. Hence, a turbulent flow is much more ordered than the disordered Euler turbulence. This is because the hydrodynamic structures at large scales are much more energetic than those at small scales (according to Kolmogorov's theory), which is not the case for the disordered Euler turbulence where the energy is equipartitioned among all Fourier modes.

For a forced turbulence, the energy spectrum $E(k)$ is maintained at a steady level. Hence, S_H of a turbulent flow is approximately constant in time. However, the coherent energy of the fluid structures are transferred to the thermal energy at microscopic scales, leading to an increase in the TE. Thus, the external force applied to the fluid flow injects hydrodynamic order that is transferred to the thermodynamic entropy at small scales. However, the thermodynamic and hydrodynamic entropies have very different properties (e.g., extensivity), hence they cannot be added. The hydrodynamic and thermodynamic disorder of a fluid system have to be separately quantified. We also remark that the TE undergoes a change via heat injection to the system or via work done by the system. Analogously, hydrodynamic entropy can be altered during the decay of turbulence or via external forcing.

In turbulence literature, a turbulent signal is contrasted with a random signal using skewness, kurtosis, and the probability distribution functions of the velocity gradients. We propose that the hydrodynamic entropy can also be used as a diagnostic tool for turbulence char-

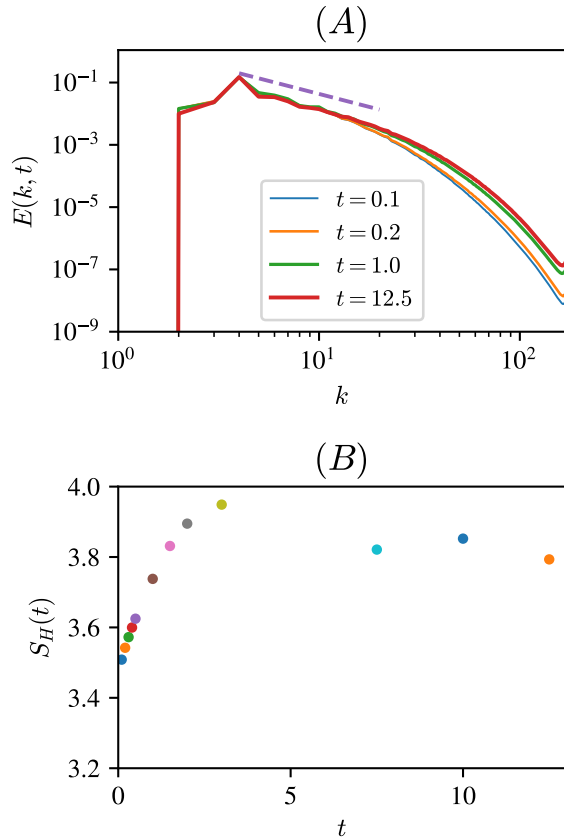


FIG. 3. For a forced hydrodynamic turbulence simulation on a 512^3 grid: (A) Plots of $E(k)$ vs. k at $t = 0.1, 0.2, 1.0$ and 12.5 eddy turnover times using colored lines with increasing thicknesses. The dashed purple line in the figure represents $k^{-5/3}$ spectrum. The figure shows that $E(k)$ at large k 's grow with time. (B) Plot of the hydrodynamic entropy $S_H(t)$ vs. t exhibits increasing entropy till $t = 5$, after which S_H flattens out (to ≈ 3.8) because the flow has reached a steady state.

acterization. If the S_H of a purported turbulent signal is far from 4, then that signal is not turbulent.

In the next section, we compute the HE for the Ising model and ϕ^4 theory.

V. HYDRODYNAMIC ENTROPY FOR SEVERAL SYSTEMS OF STATISTICAL MECHANICS

First we contrast the thermodynamic and hydrodynamic entropies of the Ising model.

A. Ising model

Consider N Ising spins each of which takes values $+\sigma$ or $-\sigma$. The Hamiltonian of the system is

$$H = -J \sum_{\langle ij \rangle} \sigma_i \sigma_j - B \sum_i \sigma_i, \quad (21)$$

where J is the coupling constant, and B is the external magnetic field. Here, the first sum is performed over the nearest neighbours, whereas the second sum is over all the spins. For the Ising model, the thermodynamic entropy is zero at zero temperature, whereas it takes the maximum value, $S_{\max} = k_B N \ln 2$, at infinite temperature. At an arbitrary temperature, we compute the entropy using Boltzmann's formulas [3].

We can also compute the hydrodynamic entropy (HE) for the Ising model as follows. The configuration of the Ising model can be specified using Fourier transform ($\hat{\sigma}_k$), which is,

$$\hat{\sigma}_k = \frac{1}{N} \sum_j \sigma_j \exp \left[-\frac{\sqrt{-1}(2\pi k j)}{N} \right] = |\hat{\sigma}_k| \exp(i\delta_k), \quad (22)$$

where $|\hat{\sigma}_k|$ and δ_k are, respectively, the amplitude and phase of the mode $\hat{\sigma}_k$. After this we define

$$p_k = \frac{|\hat{\sigma}_k|^2}{\sum_k |\hat{\sigma}_k|^2}, \quad (23)$$

and

$$S_H = - \sum_k p_k \log_2 p_k. \quad (24)$$

In the ground state, all the spins are either up ($\sigma_i = 1$) or down ($\sigma_i = -1$) that leads $p_{k=0} = 1$, and 0 for all other wavenumbers. Hence, $S_H = 0$ for the ground state. At infinite temperature, the spins are random and uncorrelated, for which

$$p_k = \frac{|\hat{\sigma}_k|^2}{\sum_k |\hat{\sigma}_k|^2} = \frac{1}{N} \text{ for } k \neq 0, \quad (25)$$

and

$$S_{H,\max} = \log_2(N), \quad (26)$$

which is the maximum possible value for S_H . At an intermediate temperature, $0 < S_H < \log_2(N)$.

Similar to Euler and hydrodynamic turbulence, S_H for the Ising system is nonextensive because $S_{H,\max} \propto \log(N)$, not N . This is one of the major differences between TE and S_H . The hydrodynamic entropy captures *multiscale* (at different length scales) order, whereas thermodynamic entropy captures *microscopic order*. Interestingly, the energy spectrum $E(\mathbf{k})$ is independent of the phase of the mode $\mathbf{u}(\mathbf{k})$. Thus, the HE is constructed

using less information of the system, yet it captures the random nature of the steady state quite well. This is one reason why S_H is less than the corresponding BE.

We remark that for the Ising model, the Shannon entropy and S_H are different even though their formulas are similar. As an example, for the maximally random Ising model, $p_1 = p_{-1} = 1/2$ for every spin that leads to

$$S_{\text{Shannon}} = N(-p_1 \log_2 p_1 - p_{-1} \log_2 p_{-1}) = N, \quad (27)$$

which is very different from S_H , which is $\log_2(N)$.

Next, we compute the hydrodynamic entropy for the ϕ^4 theory.

B. ϕ^4 theory and related equations

The *time-dependent Ginzburg-Landau (TDGL)* that describes evolution of order parameter ϕ of ϕ^4 theory is [39]

$$\partial_t \phi = \phi - \phi^3 + \nabla^2 \phi + \eta, \quad (28)$$

where η is the noise that simulates heat bath. The above system, called *Model A*, conserves $\int dx \phi(x)$. This equation is used for describing many physical phenomena, e.g., phase separation, phase transition, superconductivity, etc. It is important to note that TDGL equation is, in some sense, a hydrodynamic description of microscopic systems, such as spins.

An equilibrium solution of the TDGL equation is random ϕ with a zero mean. This solution is analogous to the random Ising spins described in Sec. V A, and its HE is $\log_2 N$, where N is the number of grid points used for discretizing Eq. (28). TDGL equation also admits two ordered equilibrium solutions, $\phi = 1$ and -1 , whose hydrodynamic entropies are zero.

TDGL equation has two nonequilibrium steady-state solutions—kink and antikink—that approach $+1$ at one end and -1 at the other end. These solutions are $\pm \tanh[(x - x_0)/\sqrt{2}]$, with size of the domain walls of the order of unity [39]. The evolution of ϕ to the kink or anti-kink or the asymptotic state, $\phi(x) = \pm 1$, are dynamic and out of equilibrium, for which we may define hydrodynamic entropy.

Following Porod's law [40, 41], the power spectrum of the kink and antikink are

$$E(k) = \frac{\mu^2}{L} k^{-2}, \quad (29)$$

where μ is the jump in ϕ across the two phases, and L is the system size. The above spectrum arises due to the discontinuity in $\phi(x)$ at the interface, and it is valid in dimensions 1, 2, and 3. Hence, the SH formula to be derived below is applicable in any dimension, as long as the $\phi(x)$ contains a kink or anti-kink. Following the same arguments as in Sec. IV, we can show that for such a system,

$$p_n = \frac{E_n}{E} = A(k_n L)^{-1} = A\lambda^{-n}, \quad (30)$$

and the hydrodynamic entropy is given by Eq. (19) with $\alpha = 1$. See Fig. 4 for an illustration of $S_H(G)$ for $\lambda = 1.2, 1.3, 1.4, 1.5$. For large G , S_H of a coarsening system is

$$S_H \approx \frac{\log_2 \lambda}{\ln \lambda} - \log_2(A) = \frac{\log_2 \lambda}{\ln \lambda} - \log_2[\lambda \ln(\lambda)]. \quad (31)$$

The asymptotic values of S_H for $\lambda = 1.2, 1.3, 1.4, 1.5$ are 3.64, 2.99, 2.53, and 2.16 respectively, which are presented as dashed red lines in Fig. 4. In addition, the TDGL equation admits a random state, whose $S_H = \log_2 N$, and two other asymptotic states, $\phi = \pm 1$, for whom $S_H = 0$. Note that the maximum TE for the random state is $O(N)$. Hence, the HE of the TDGL equation is nonextensive because it is never proportional to N .

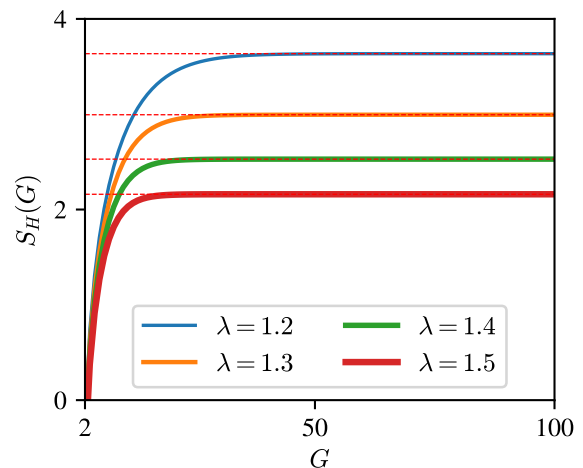


FIG. 4. For kink-antikink pairs of coarsening, plots of hydrodynamic entropy $S_H(G)$ vs. G computed using the analytical formula [Eq. (19)] with $\alpha = 1$ and $\lambda = 1.2, 1.3, 1.4, 1.5$ using colored lines of increasing thicknesses. The asymptotic values [Eq. (20)] for the four λ 's are 3.64, 2.99, 2.53, and 2.16 respectively (horizontal dashed lines).

We illustrate the evolution of HE using a direct numerical simulation of TDGL equation. We analyze the numerical data generated by Verma *et al.* [41], who simulated the TDGL equation using finite difference method in a one-dimensional (1D) periodic box of size $L = 100$ with a grid resolution of 1024. They took the time step $\Delta t = 0.001$ that satisfies the Courant–Friedrichs–Lewy (CFL) or linear-stability condition [41]. They evolved a biased initial state ($\langle \phi(x, t=0) \neq 0 \rangle$) from $t = 0$ to $t = 9.8$. In Fig. 5(A) we illustrate the evolution of $\phi(x, t)$ from a random state (blue curve) to the asymptotic state, $\phi(x) = 1$.

For the above $\phi(x, t)$, the corresponding energy spectra ($E(k)$) and hydrodynamic entropies ($S_H(t)$) are exhibited in Fig. 5(B,C) respectively. As shown in Fig. 5(B), the initial $E(k, t)$ are spread out among a wide range

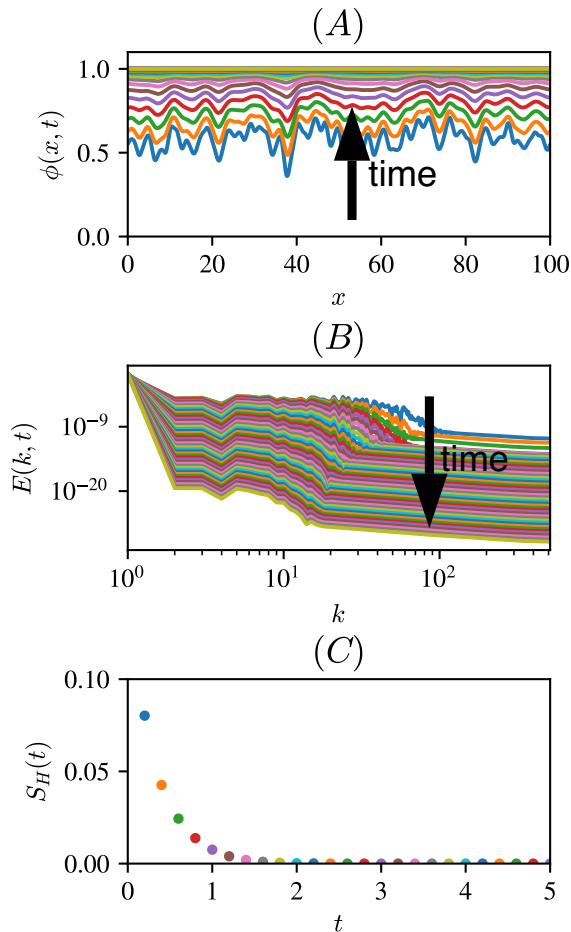


FIG. 5. For a simulation of TDGL equation with biased initial condition ($\langle \phi(x, t=0) \rangle \neq 0$): (A) Plots of $\phi(x, t)$ vs. x from $t = 0.1$ to 9.8. $\phi(x, t)$ starts from the blue-colored configuration and increases to $\phi(x, t) = 1$ near $t \approx 3$. (B) The respective energy spectrum $E(k, t)$ vs. k ; $E(k, t)$ spreads out initially, but it tends to concentrate at lower k 's. Asymptotically, $E(k)$ is nonzero only for $k = 0$. (C) Plot of hydrodynamic entropy $S_H(t)$ up to $t = 5$ shows that $S_H(t)$ decreases asymptotically to zero.

of wavenumbers. With time, $E(k)$ for large k 's dissipates more strongly than those for small k 's [41]. Consequently, $E(k, t)$ becomes more skewed towards small wavenumbers. Hence, the HE of the system decreases monotonically with time, as illustrated in Fig. 5(C). The HE of the asymptotic state is zero.

For an unbiased initial condition, the TDGL equation evolves to one or more kink-antikink pairs. The HE for the asymptotic state would be given by Eq. (31). Following similar analysis as above, we can numerically verify these results. In addition, we can also compute the hydrodynamic entropy for model B [42], and expect the behaviour to be similar. To maintain focus on the main

theme, we do not present these results here.

We also remark that the emergence of ordered states— $\phi = \pm 1$ or kink/antikink—in 1D TDGL equation does not contradict *Mermin-Wagner theorem*, according to which long-range order (LRO) does not exist in 1D and 2D *equilibrium* systems with short-range interactions. Nonequilibrium nature of turbulent flows and TDGL equation invalidates the arguments of Mermin-Wagner theorem. Note that Toner and Tu [43] observed flocking and related long-range ordered states in 2D active matter.

The above examples contrast the hydrodynamic and thermodynamic entropies. In the next section, we summarize our results.

VI. DISCUSSIONS AND CONCLUSIONS

We start this paper with Prigogine [12]'s motivation for the emergence of the dissipative structures in Rayleigh-Bénard convection. In this paper we argue that such convective patterns, which are more ordered than conduction profile, require new measures for disorder quantification (other than thermodynamic entropy). In this paper, we show that hydrodynamic entropy (HE) captures such a multiscale order/disorder.

In this paper, we compute the hydrodynamic entropies of Euler and hydrodynamic turbulence, TDGL equation, and Ising spins. Via these examples, we show that the HE is nonextensive, and it differs significantly from the thermodynamic entropy (TE). We summarize some of the important properties of HE as follows:

1. HE is a measure of multiscale and macroscopic disorder. In contrast, TE captures microscopic disorder (single-scale phenomena). However, there is an exception: TE capture multiscale disorder near second-order phase transition.
2. TE is an extensive quantity, that is, it depends on the system size. However, HE is nonextensive. For example, the HE of equilibrium Euler turbulence is $\log_2 M$, where M is the grid size. The HE of a turbulent flow is even lower (between 3 and 4), and it is dominated by the large-scale structures.
3. Since TE and HE have very different properties, we cannot add them to compute the total entropy of a system. We use the respective entropies to specify the disorder at different scales. This is in the same spirit why we ignore quantum fields and fundamental particles—quarks and electrons—while describing gases and liquids.

Many natural processes are out of equilibrium and multiscale. Some of the popular examples are plasma turbulence [44], financial systems [18], ecological systems, electroencephalogram (EEG) [19], electrocardiogram (ECG) [20], voltage-dependent anion channels [45],

etc. These systems exhibit power-law spectrum, somewhat similar to turbulence. Hence, we expect their HE to have similar properties. Tsallis entropy [46] appears to describe order of these systems satisfactorily (see Appendix A). For quantum systems, quantification of order and entanglement remains a challenge, and it is an active area of research. von Neumann entropy, entanglement entropy, and information entropy are popular measures in this field [47] (see Appendix A). For quantum systems, construction of hydrodynamic entropy, and its comparison with other entropies will be an interesting exercise.

Among the entropies discussed in Appendix A, only Tsallis entropy is nonextensive, and the rest are extensive. Note that HE too is nonextensive. Hence, a detailed comparison between the Tsallis entropy and HE will be useful. In addition, the formula for HE, Eq. (4), resembles Shannon entropy formula. But, HE and Shannon entropy are very different, as we illustrate in Sec. V A. This paper brings out similarities and dissimilarities between various entropies. Still, further comparison between them is required.

Researchers often employ particle-based simulations, e.g, molecular dynamics (MD), to study microfluids, chemical reactions, turbulence, and interacting many-particle systems [48]. Thermodynamic entropy is useful for such systems when they are in equilibrium or near equilibrium. However, TE does not capture the order accurately in MD simulations involving thermal convection, turbulence [49], granular matter [50], or strongly-interacting plasmas [51]. We believe that HE computed using coarse-grained hydrodynamics may be useful for quantifying order in such systems. We hope that such exercise will be performed in future.

Nonequilibrium systems typically exhibit energy transfers across scales. In hydrodynamic turbulence, the multiscale energy transfer is proportional to the third-order structure function or triple-order correlation of Fourier modes [25, 32, 52]. Hydrodynamic entropy ignores the phases of the Fourier modes, hence it can not provide information on the energy transfers or phase correlations. The *phase entropy* [53], which is used for quantifying *phase synchronization*, may be useful for the analysis and global measure of multiscale energy transfers.

We emphasize that the multiscale framework provides valuable insights into the nonequilibrium systems. For example, multiscale energy transfers can be employed to break the time reversal symmetry in nonequilibrium driven systems [26, 30]. Hydrodynamic entropy, an important quantity in the multiscale framework, could complement past works in this field.

Acknowledgements : The authors thanks Riddhi Bandyopadhyay, Anurag Gupta, and Adhip Agarwal for useful discussions; and Abhishek Jha and Pradeep Yadav for providing simulation data. MKV gratefully acknowledges the support from Science and Engineering Research Board, India, for the J. C. Bose Fellowship (SERB /PHY/2023488) and for the grants

SERB/PHY/20215225 and SERB/PHY/2021473. RS thanks IIT Kanpur for the visiting faculty position in 2023 and 2024, during which this work was done.

Appendix A: Various Entropies Used in Physics

In this Appendix, we summarize thermodynamic entropy, Shannon entropy, von Neumann entropy, and Tsallis entropy. In the main text, we compare these entropies with the hydrodynamic entropy.

Thermodynamic entropy: In statistical mechanics, if a system has W microstates or configurations that occur with equal probability, then the *configuration entropy* or *Boltzmann entropy* is given by $S = k_B \log W$, where k_B is Boltzmann constant [4]. At zero temperature (T), $W = 1$ and $S = 0$, which is the minimum entropy for the system. However, at infinite temperature, the system is completely random and the entropy is maximal. For the random Ising system with N spins, $W = 2^N$ and $S = k_B \log W = k_B N \log 2$.

The thermodynamic entropy of an ideal gas with N particles in a box of volume V with a total energy of E is [3]

$$S = Nk_B \left[\log \frac{V}{N} + \frac{3}{2} \log \frac{4\pi m E}{3N h^2} + \frac{5}{2} \right], \quad (\text{A1})$$

where h, k_B are the Planck and Boltzmann constants, and m is the mass of each particle. The above thermodynamic entropies are extensive because they are proportional to N .

According to Gibbs [2], a macrostate of a thermodynamic system is combination of microstates. If probability of i^{th} microstate is p_i , then the Gibbs entropy is

$$S_G = -k_B \sum_i p_i \log p_i. \quad (\text{A2})$$

At a finite temperature, $S = -\partial F/\partial T$ where $F = -k_B T \log Z$ with $Z = \sum_C \exp(-\beta E_C)$. Since $\log Z$ is proportional to the system size, the thermodynamic entropy S is extensive [3].

Shannon entropy: Shannon entropy [14] is very useful in computer science and electrical engineering, in particular for data compression and transmission. Imaging an string of n random symbols, where the random symbol x occurs with probability p_x . Then, the Shannon entropy is defined as

$$S = - \sum_x p_x \log_2 p_x. \quad (\text{A3})$$

If x has n possible outcomes that are equally probable, then $p_x = 1/n$ for all n , and

$$S = S_{\max} = - \sum_x \frac{1}{n} \log_2 \frac{1}{n} = \log_2(n). \quad (\text{A4})$$

When the probabilities for the outcomes are unequal, it is easy to show that $S < S_{\max}$. Note that the Shannon entropy is extensive.

von Neumann entropy: von Neumann entropy [47], an extension of Gibbs entropy, is useful for entropy computation of quantum systems. It is

$$S = -\text{Tr}(\hat{\rho} \log \hat{\rho}), \quad (\text{A5})$$

where $\hat{\rho}$ is the density matrix,

$$\hat{\rho} = \eta_j |j\rangle\langle j| \quad (\text{A6})$$

with $|j\rangle$ as the basis state. When $|j\rangle$'s are the eigenvectors of the system, then

$$S = -\sum_j \eta_j \log(\eta_j), \quad (\text{A7})$$

which is same as the Gibbs entropy.

For a quantum system with N qubits of spin 1/2, the Hilbert space is 2^N dimensional. If each quantum state has equal probability, then $\eta_j = 2^{-N}$ for all j 's that leads

to

$$S = N \log 2, \quad (\text{A8})$$

which is the maximum value of the von Neumann entropy. Since $S \propto N$, the von Neumann entropy is extensive.

Tsallis entropy: Tsallis entropy [46], S_q , an extension of Boltzmann and Gibbs entropies, provides expectation of q-logarithm of a distribution:

$$S_q = k \frac{1 - \sum_{i=1}^q p_i^q}{q-1} \quad (\text{A9})$$

where $\sum_i p_i = 1$, q is a real parameter, and k is a positive constant. When $q \rightarrow 1$, $S_q \rightarrow -k \sum_i p_i \log_2 p_i$, which is Gibbs entropy. Note that Tsallis entropy is not additive, and hence nonextensive (except when $q \rightarrow 1$). Tsallis entropy finds application in chaos theory, dusty plasma, spin glass relaxation, etc. Note that Tsallis entropy measures disorder at single-scale, whereas hydrodynamic entropy captures multiscale disorder. Still, it is important to compare the nonextensive features of the two entropies.

The other important entropies employed in physics are entanglement and information entropies [47], black hole entropy [54], and phase entropy [53]. However, we do not discuss them here because they are beyond the scope of this paper.

-
- [1] L. Boltzmann, in *The kinetic theory of gases: an anthology of classic papers with historical commentary* (World Scientific, 2003) pp. 262–349.
- [2] J. W. Gibbs, *Elementary principles in statistical mechanics* (Dover Publications, New York, 1960).
- [3] K. Huang, *Statistical Mechanics*, 2nd ed. (John Wiley & Sons, 1987).
- [4] L. D. Landau and E. M. Lifshitz, *Statistical Physics*, 3rd ed. (Elsevier, Oxford, 1980).
- [5] K. G. Wilson and J. Kogut, Phys. Rep. **12**, 75 (1974).
- [6] S. Chandrasekhar, *Hydrodynamic and Hydromagnetic Stability* (Oxford University Press, Clarendon, 1961).
- [7] G. K. Vallis, *Atmospheric and Oceanic Fluid Dynamics* (Cambridge University Press, Cambridge, 2006).
- [8] P. Manneville, *Instabilities, Chaos and Turbulence* (Imperial College Press, London, 2004).
- [9] M. K. Verma and S. Chatterjee, Phys. Rev. Fluids **7**, 114608 (2022).
- [10] L. D. Landau and E. M. Lifshitz, *Fluid Mechanics*, 2nd ed. (Elsevier, Oxford, 1987).
- [11] C. Cichowlas, P. Bonaïti, F. Debbasch, and M. E. Brachet, Phys. Rev. Lett. **95**, 264502 (2005).
- [12] I. Prigogine, Science **201**, 777 (1978).
- [13] I. Prigogine, Nobel Lecture (1977).
- [14] C. E. Shannon, Bell Labs Tech. J. **27**, 379 (1948).
- [15] A. Golan and J. Harte, PNAS **119**, e2119089119 (2022).
- [16] S. Mishra and B. M. Ayyub, Risk Analysis **39**, 2160 (2019).
- [17] R. Rajaram, B. Castellani, and A. N. Wilson, Complexity **2017**, 1 (2017).
- [18] R. Zhou, R. Cai, and G. Tong, Entropy **15**, 4909 (2013).
- [19] G. Deco and M. L. Kringelbach, Cell Reports **33**, 108471 (2020).
- [20] A. Asgharzadeh-Bonab, M. C. Amirani, and A. Mehri, Biocybernetics and Biomedical Engineering **40**, 691 (2020).
- [21] D. Clark, L. Tarra, and A. Berera, Phys. Rev. Fluids **5**, 064608 (2020), 2003.08159.
- [22] N. Aubry, R. Guyonnet, and R. Lima, J. Stat. Phys. **64**, 683 (1991).
- [23] J. L. Lebowitz, Physica A **194**, 1 (1993).
- [24] S. A. Orszag, in *Les Houches Summer School of Theoretical Physics*, edited by R. Balian and J. L. Peube (Gordon Breach, New York, 1973) p. 235.
- [25] S. B. Pope, *Turbulent Flows* (Cambridge University Press, Cambridge, 2000).
- [26] M. K. Verma, Eur. Phys. J. B **92**, 190 (2019).
- [27] T. D. Lee, Quart. Appl. Math. **10**, 69 (1952).
- [28] R. H. Kraichnan, J. Fluid Mech. **59**, 745 (1973).
- [29] M. Lesieur, *Turbulence in Fluids* (Springer-Verlag, Dordrecht, 2008).
- [30] M. K. Verma, Phil. Trans. R. Soc. A. **378**, 20190470 (2020).
- [31] M. K. Verma, S. Chatterjee, A. Sharma, and A. Mohap-

- atra, Phys. Rev. E **105**, 034121 (2022).
- [32] A. N. Kolmogorov, Dokl Acad Nauk SSSR **30**, 301 (1941).
- [33] E. B. Gledzer, Dokl Acad Nauk SSSR **209**, 1046 (1973).
- [34] L. Biferale, Annu. Rev. Fluid Mech. **35**, 441 (2003).
- [35] A. G. Chatterjee, M. K. Verma, A. Kumar, R. Samtaney, B. Hadri, and R. Khurram, J. Parallel Distrib. Comput. **113**, 77 (2018).
- [36] S. Sadhukhan, M. K. Verma, R. Stepanov, F. Plunian, and R. Samtaney, Phys. Rev. Fluids **4**, 84607 (2019).
- [37] C. Canuto, M. Y. Hussaini, A. Quarteroni, and T. A. Zang, *Spectral Methods in Fluid Dynamics* (Springer-Verlag, Berlin Heidelberg, 1988).
- [38] M. K. Verma, A. G. Chatterjee, R. K. Yadav, S. Paul, M. Chandra, and R. Samtaney, Pramana-J. Phys. **81**, 617 (2013).
- [39] P. M. Chaikin and T. C. Lubensky, *Principles of Condensed Matter Physics* (Cambridge University Press, New York, 2000).
- [40] G. Porod, in *Small angle X-ray scattering*, edited by O. Glatter and O. Kratky (Academic Press, New York, 1982) p. 35.
- [41] M. K. Verma, R. Agrawal, P. K. Yadav, and S. Puri, Phys. Rev. E **107**, 034207 (2023).
- [42] S. Puri and V. Wadhawan, eds., *Kinetics of Phase Transitions* (CRC Press, Boca Raton, FL, 2009).
- [43] J. Toner and Y. Tu, Phys. Rev. E **58**, 4828 (1998).
- [44] W. H. Matthaeus, Y. Yang, M. Wan, T. N. Parashar, R. Bandyopadhyay, A. Chasapis, O. Pezzi, and F. Valentini, ApJ **891**, 0 (2020).
- [45] M. K. Verma, S. Manna, J. Banerjee, and S. Ghosh, EPL **76**, 1050 (2006).
- [46] C. Tsallis, *Introduction to nonextensive statistical mechanics: approaching a complex world* (Springer, 2009).
- [47] W. H. Zurek, Rev. Mod. Phys. **75**, 715 (2003).
- [48] G. A. Bird, *Molecular Gas Dynamics and the Direct Simulation of Gas Flows* (Clarendon, Oxford, 1994).
- [49] M. A. Gallis, N. P. Bitter, T. P. Koehler, J. R. Torczynski, S. J. Plimpton, and G. Papadakis, Phys. Rev. Lett. **118**, 064501 (2017).
- [50] P. G. de Gennes, Rev. Mod. Phys. **71**, S374 (1999).
- [51] R. Wani, M. Verma, and S. Tiwari, Phys. Plasmas **31**, 082306 (2024).
- [52] M. K. Verma, *Energy transfers in Fluid Flows: Multiscale and Spectral Perspectives* (Cambridge University Press, Cambridge, 2019).
- [53] Y. Kuramoto, *Chemical Oscillations, Waves, and Turbulence* (Springer, New York, 1984).
- [54] S. B. Giddings, Phys. Today **66**, 30 (2013).